Effect of gelation pH on whey protein aerogel properties

Journal of Sol-Gel Science and Technology (2026)119:20
https://doi.org/10.1007/s10971-026-07221-0

ORIGINALPAPER

Effect of gelation pH on whey protein aerogel properties

Umair Ashraf[1] · Marta Gallo[1] · Luigi Manna[1] · Francesca Bosco[1] · Barbara Onida[1]

Received: 8 January 2026 / Accepted: 13 July 2026

Abstract

Due to their bioinspired self-assembly and biocompatibility, protein-based aerogels have drawn growing interest in biomedical applications. With its excellent gelling and self-assembly properties, whey protein isolate (WPI) represents a promising source for the fabrication of biodegradable and homogeneous tunable aerogels. Gelation pH has a significant impact on the morphological homogeneity of protein biomaterials, which is essential for controlling tissue-implant interactions. In this study, WPI aerogels were produced without gelation-induced agents (followed by a supercritical CO_2 drying process), and the effect of the gelation pH was investigated by varying its value from 2 to 11. Aerogels with a high fluid absorption capacity (~ 760%), specific surface area (312 $m^2 . g^{-1}$), and pore volume (1.02 $cm^3 . g^{-1}$) were obtained by gelation at neutral to mildly alkaline conditions (pH 7-8.5). Because of their excellent fluid absorption capacity, these aerogels have the potential to be a biocompatible wound dressing. On the other hand, aerogels from acidic gelation conditions (pH < 3) dissolved or disintegrated during fluid absorption. Monolithic aerogels were obtained by increasing the gelation pH. However, as the gelation pH approached the WPI isoelectric region (pH 4-6) or extreme alkaline pH (pH ≥ 9), aerogels presented low specific surface area and fluid absorption capacity. Overall, this study confirms that gelation pH affects the structural and functional properties of WPI aerogels and offers a systematic investigation of the effect of gelation pH on the resulting aerogels.

Graphical Abstract

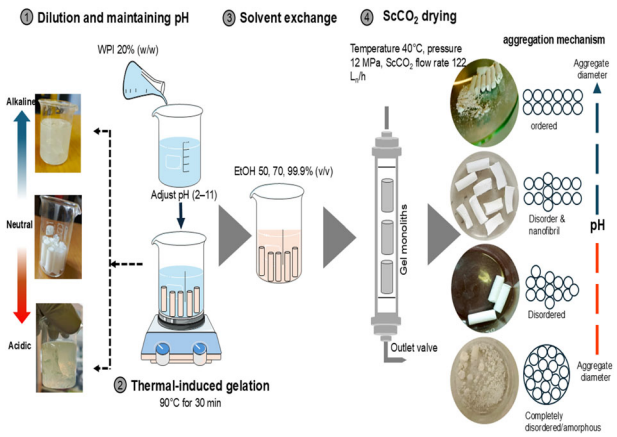

Keywords Whey protein isolate aerogels · Gelation pH · Biomaterials · Wound healing

✉ Marta Gallo
marta.gallo@polito.it

[1] Department of Applied Science and Technology (DISAT), Politecnico di Torino, Turin, Italy

Published online: 23 July 2026

Research Highlights

- Crosslinker-free synthesis of whey protein isolate (WPI) aerogels achieved via sol-gel chemistry and supercritical CO_2 drying.
- The gelation pH of WPI affects the aerogel properties.
- The highest surface area and stability were obtained at neutral to mildly alkaline gelation pH.
- Aerogels gelled at pH 7 exhibit liquid absorption values apt for wound healing.

1 Introduction

Aerogels are a class of materials known for their high porosity and large specific surface area. Aerogels are typically produced through sol-gel chemistry followed by a drying process, resulting in a three-dimensional network with high pore volume and low density [1]. Aerogels can be fabricated from organic macromolecules [2–4], inorganic precursors [5], or combinations of organic and inorganic molecules [6]. Biopolymeric aerogels derived from polysaccharides (cellulose, chitosan, alginate, starch, pectin, carrageenan) [7, 8] and proteins (collagen, gelatin, silk fibroin, whey protein) [1] offer a unique combination of biocompatibility, biodegradability, and intrinsic bioactivity highly desirable for biomedical purposes. In addition, in biomedical applications, protein-based biomaterials exhibit innate biological activities and reduced immunogenic properties [9].

Among the different proteins that can be turned into aerogels, whey protein isolate (WPI) is of particular interest. WPI is a by-product of the dairy industry, consisting of a complex protein. Valorizing this agri-food waste stream into value-added biomaterials addresses both economic and sustainability challenges. Previous studies have highlighted the potential of WPI-based biomaterials, such as hydrogels prepared via sol-gel chemistry, for drug encapsulation, wound treatment, and tissue engineering [10–12]. WPI-based aerogels produced via supercritical CO_2 drying or freeze-drying [13] have potential extensive applications in food as a solid saturated fat replacer [14, 15] and packaging materials [16, 17], in drug and bioactive compounds delivery [18–20], tissue engineering [21], and environmental and water remediation [22–24]. However, despite promising functional properties for diverse applications, a comprehensive understanding of how precursor gelation conditions control the final aerogel properties and performance remains limited.

Among the various parameters that influence WPI gelation in sol-gel synthesis, pH and temperature play a critical role in determining the hydrogel structures [25] and the resulting microstructure of aerogels [26]. Heating induces gelation by affecting protein tertiary structures, promoting intermolecular disulfide crosslinking and hydrophobic aggregation, depending on pH [27–29]. Regarding pH, it is reported in the literature that hydrogels produced near the isoelectric point (pH~4.9) consist of an opaque gel made of small, spherical, and dense aggregates. Instead, gels formed at high acidic or alkaline pH are transparent with fine and homogeneous aggregates [30, 31]. Whey protein hydrogels formed near the isoelectric point showed lower porosity and exhibited high water retention and elasticity [32–34].

Concerning the influence of gelation pH on the properties of resulting aerogels, WPI-based aerogels for ketoprofen delivery were synthesized at different gelation pH values using the sol-gel route [20]. The gelation pH strongly influenced the textural properties of the resulting aerogels. Aerogels produced near the isoelectric point (pH 4.5) exhibited the lowest surface area (14 ± 10 $m^2 . g^{-1}$), due to extensive particulate aggregation and reduced mesoporosity. In contrast, aerogels formed under highly acidic conditions (pH 1.5) displayed the highest surface area (420 ± 80 $m^2 . g^{-1}$), while those prepared under alkaline conditions (pH 10) also exhibited high surface area (390 ± 70 $m^2 . g^{-1}$). These findings reinforce the strong dependence of WPI aerogel porosity and pore volume on pH-tuned aggregation behavior.

In another study, WPI aerogel particles were synthesized via sol-gel processing at gelation pH 5.7 followed by either supercritical or freeze drying, to investigate their oleogelation ability. The resultant freeze-dried aerogels exhibited lower dispersibility in water than supercritical-dried aerogels, confirming that freeze-dried aerogels had more intense aggregation [15]. However, no information about the microstructural and textural properties of the resulting aerogels was reported in the study.

For oral delivery applications, WPI-sodium caseinate aerogel microparticles have been developed and evaluated for in-vitro digestion performance. These aerogels displayed the highest specific surface area (~ 380–420 $m^2 . g^{-1}$) when gelation occurred at highly acidic and alkaline pH, enabling fish oil loading capacities up to 63% (w/w). These findings highlighted the critical role of gelation pH in tuning porosity and loading efficiency of protein-based aerogels [35]. WPI aerogels have also been explored as a zinc micronutrient carrier. In this case, aerogels were synthesized at gelation pH 1.0 and 3.0 via the sol-gel method followed by supercritical CO_2 drying. The aerogels obtained at gelation pH 1.0 had a specific surface area of 160 ± 100 $m^2 . g^{-1}$, while the aerogels obtained at gelation pH 3.0 display no detectable surface area [19].

In the case of WPI aerogels, most studies have primarily focused on gelation pH effects on the microstructure and its influence on functional properties such as oleogelation behavior, in vitro digestion dynamics, bioactive loading, and release kinetics. These investigations collectively highlight the critical role of pH during protein assembly in determining the physicochemical properties of WPI aerogels across food, nutraceutical, and pharmaceutical applications.

Despite well-established WPI protein chemistry, systematic studies correlating a broad gelation pH range (2 to 11) to the structural and functional properties of WPI aerogels remain limited, particularly for wound treatment. The objective of this study is to better understand the correlation between gelation pH and the resulting aerogel characteristics. We thoroughly examined the synthesis of WPI-aerogels in a wide pH range (2 to 11) without the incorporation of crosslinking agents. Distinct morphological transitions that correlate with pH are revealed by structural and physical characterization, offering new insights for designing function-specific protein aerogels intended for biomedical use.

2 Materials and methods

2.1 Material

WPI Milei®90 (WPI; 93% protein, 2.7% ash, 0.2% fat, and lactose 1.1%; pH 6.2) was kindly supplied by Milei® GmbH (Leutkirch, Germany). Hydrochloric acid (HCl) and sodium hydroxide (NaOH) (Sigma-Aldrich®, Merck, Germany) were used for pH adjustment. Absolute anhydrous ethanol (analytical grade, Merck) was used for solvent exchange. Deionized water was obtained from a LiChrosolv® purification system (Merck, Billerica, MA, USA).

2.2 Preparation of WPI-hydrogel

WPI hydrogels were prepared following the method of Manzocco [13] with minor modifications. Briefly, WPI (20 g) was dissolved in deionized water (60 mL) under continuous stirring at room temperature for 4 h to obtain a homogeneous solution. The stock solutions were stored overnight at 4 °C to ensure complete protein hydration. After dilution to a final concentration of 20% (w/w), the solution temperature was maintained at 20 °C, and pH was measured using a calibrated pH meter (Hanna HI 5221, USA). The desired pH values (ranging from 2 to 11) were adjusted using a 2 M HCl solution or a 2 M NaOH solution. The pH-adjusted WPI suspensions were transferred into glass tubes ($l = 22$ mm, $d = 6.5$ mm, $t = 1.5$ mm), serving as molds, as illustrated in Fig. 1. Gelation was induced by heating the filled tubes at 90 °C for 30 min in a temperature-controlled water bath. The resulting hydrogels were cooled to room temperature, gently taken out of glass tubes, and washed with deionized water to eliminate unreacted residues. Hydrogel dimensions were measured using a precision caliper.

2.3 Supercritical CO_2 dried WPI-aerogel

The hydrogel cylinders were converted into alcogels following the procedure described by Betz [20]. Water in the hydrogel matrix was gradually replaced with ethanol through stepwise solvent exchange using ethanol concentrations of 50, 70, 95, and 99.8% (v/v), each after 24 h. After completing solvent exchange, the alcogels were subjected to supercritical CO_2 drying ($ScCO_2$ drying). Drying was performed in a stainless-steel cylindrical autoclave (internal diameter: 1.4 cm; length: 22 cm; internal volume: ~ 34 cm^3) (DISAT, Politecnico Di Torino) operating at 12 MPa, and 40 °C, with a continuous supercritical CO_2 flow rate of 120 L_n/h for 4–6 h. The resulting aerogels were designated according to the pH at which the precursor hydrogels were formed: AeroWPI-2, AeroWPI-3, AeroWPI-4, AeroWPI-5, AeroWPI-6, AeroWPI-7, AeroWPI-7.5, AeroWPI-8, AeroWPI-8.5, AeroWPI-9, AeroWPI-10, and AeroWPI-11. Aerogels prepared at highly acidic gelation pH (pH ≤ 3) fragmented or cracked during $ScCO_2$ drying; samples gelled between pH 4 and 7 formed intact monoliths with surface textures ranging from slightly dusty to smooth, while aerogels produced at high alkaline gelation (pH ≥ 8) were hard and brittle.

2.4 Aerogel characterization

2.4.1 Physical properties

The physical properties of WPI aerogels obtained at different gelation pH values were evaluated.

Bulk density (ρ) of the WPI aerogels was determined by measuring the aerogel mass (m) and geometric volume (V) using the following Eq. (1):

$$\rho\left(g\ cm^{-3}\right) = \left(\frac{m}{V}\right) \tag{1}$$

Volume shrinkage (S_v) of WPI aerogels was calculated as the percentage reduction between alcogel ($V_{alcogel}$) and corresponding aerogel volumes after $ScCO_2$ drying ($V_{aerogel}$) using Eq. (2):

$$Sv = \left(\frac{V_{alcogel} - V_{aerogel}}{V_{alcogel}}\right) x100\% \tag{2}$$

Porosity (ε) was measured via the liquid displacement method with absolute ethanol (~ 0.789 g·cm^{-1}), which readily penetrates the pore network without swelling or dissolving the protein matrix. Aerogel samples ($h = 8\ mm$, $d = 5\ mm$) were weighed dry (W_1), immersed in absolute ethanol for 5 min, removed, gently blotted, and reweighed

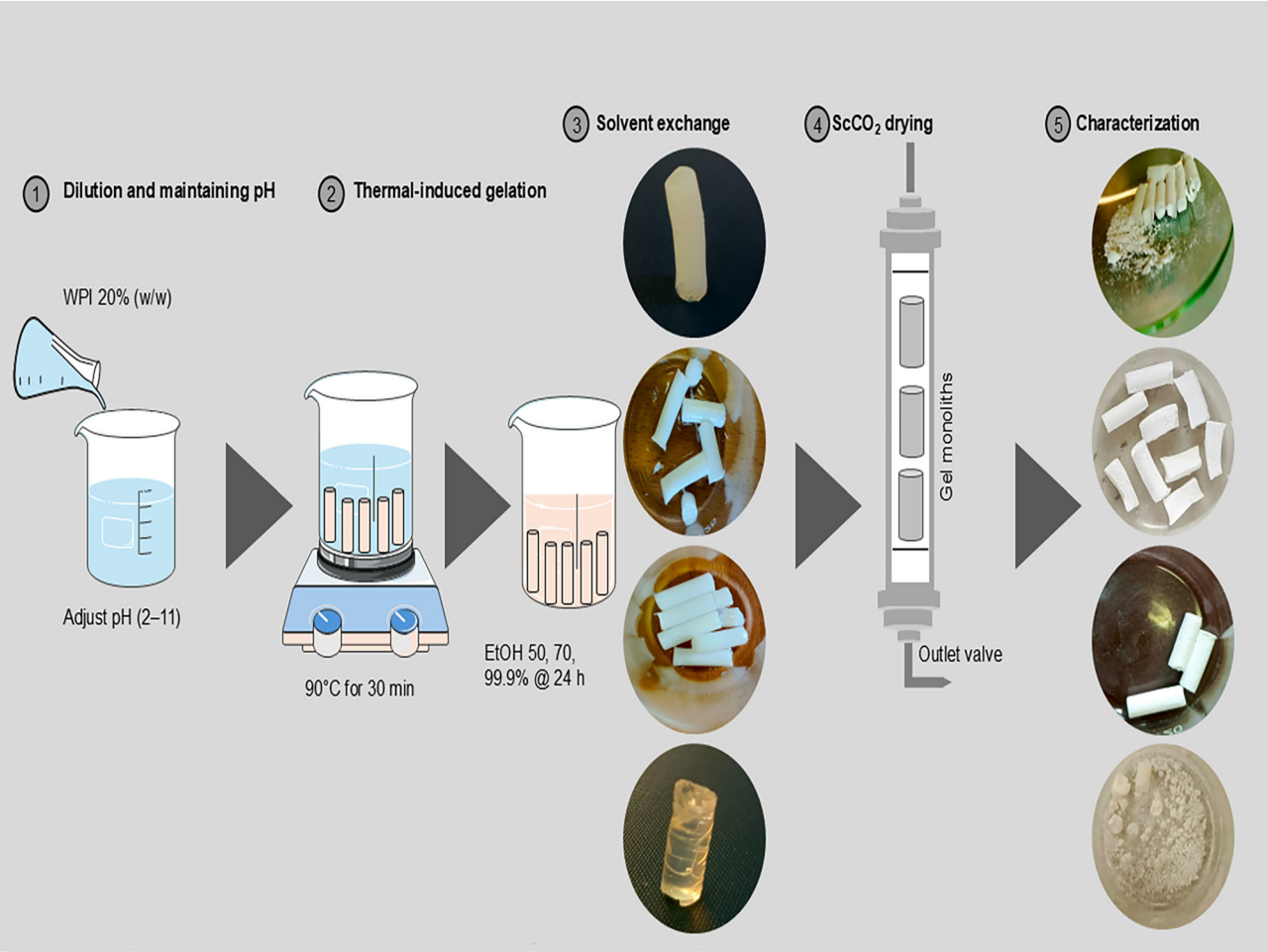

Fig. 1 Preparation of WPI-aerogels

(W_2). Porosity was calculated as Eq. (3):

$$\varepsilon = \left(\frac{W_2 - W_1}{\rho_{Eth}\, x\, V_{scaffold}}\right) x100\% \quad (3)$$

2.4.2 N_2 adsorption-desorption isotherms

Textural properties were characterized by nitrogen adsorption–desorption isotherms using a Micromeritics ASAP 2020 Plus Physisorption analyzer (Micromeritics, Norcross, GA, USA). Samples were outgassed at 333 K for 20 h prior to analysis. Specific surface area (SSA) was calculated using the Brunauer-Emmett-Teller (BET) model within the IUPAC-recommended relative pressure range ($P/P_o = 0.05$–0.30) [36]. BET plots exhibited excellent linearity ($r > 0.999$) and C-constants > 80, confirming the reliability of the model application. Mean pore diameter (D_p) and total pore volume (V_T) were derived from the Barrett-Joyner-Halenda (BJH) method.

2.4.3 Determination of zeta-potential and swelling degree of WPI aerogels

Zeta potential (ζ) was measured to evaluate surface charge and electrostatic stability. Aerogels were dispersed in 1.0 mM KCl (0.1 mg· mL^{-1}) and analyzed at 20 °C with an equilibration time of 120 s using a Litesizer ™ 500 (Anton Paar GmbH, Austria). Electrophoretic mobility was converted to ζ-potential using the Smoluchowski approximation [22].

Swelling behavior was measured following a modified DIN EN ISO 175:2000 [22]. Dried aerogels ($l = 5$ mm, $d = 5$ mm, weight (W_1)) were immersed in deionized water at room temperature for 24 h. The swollen samples were blotted to remove surface liquid and weighed (W_3), then dried at 65 °C for 3–4 h and reweighed (W_4). The degree of swelling (DS) was calculated as Eq. (4):

$$DS = \left(\frac{W_3 - W_4}{W_4}\right) x100\% \quad (4)$$

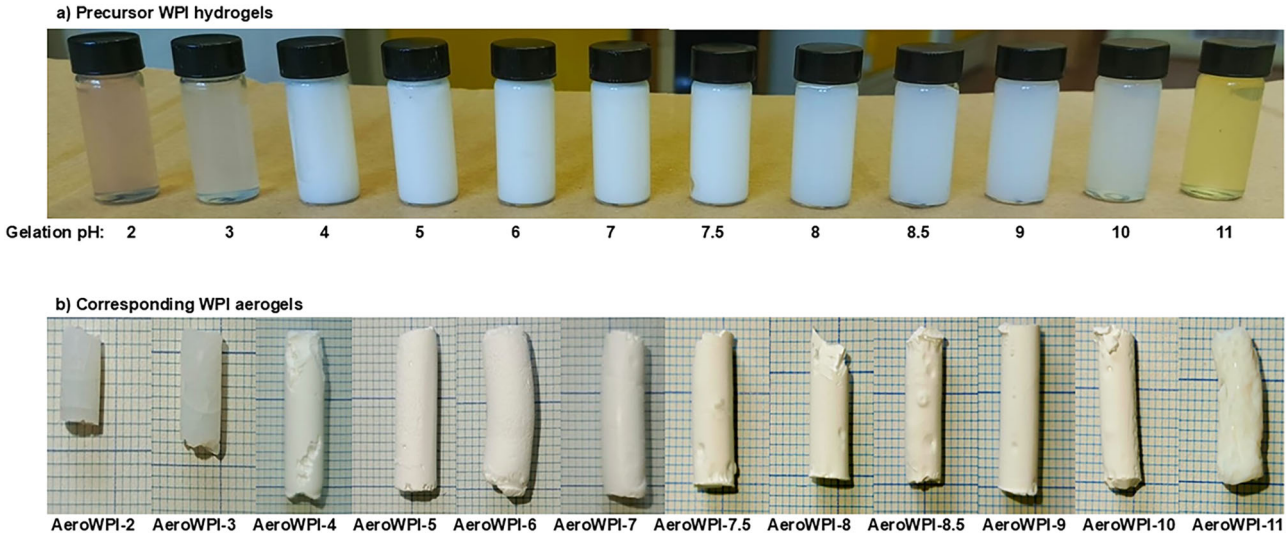

Fig. 2 WPI hydrogels prepared at various pH values (**a**) and corresponding aerogels (**b**)

2.4.4 Liquid absorption capacity

Liquid absorption capacity was evaluated using PBS (pH 7.4). Samples ($l = 5$ mm, $d = 5$ mm) were weighed (W_1), immersed in 10 mL PBS for 2, 4, 12, 24, and 48 h, then blotted and reweighed (W_5). The absorption (%) was calculated as Eq. (5):

$$Liquid\ absorption = \left(\frac{W_5 - W_1}{W_1}\right) x100\% \quad (5)$$

2.4.5 Physicochemical properties of selected aerogels (AeroWPI-7 & 8.5)

Microstructural analysis was performed using a field-emission scanning electron microscope (ZEISS Merlin, Oxford Instruments, Abingdon-on-Thames, UK). Aerogel powder was spread on aluminum stubs and sputter-coated with a 10 nm platinum layer prior to imaging. Micrographs were taken under vacuum at ambient temperature with an acceleration voltage of 20 kV.

Fourier Transform Infrared (FTIR) spectra were recorded using an Invenio S spectrometer (Bruker, Germany) in the range of 4000-400 cm^{-1} at a resolution of 2 cm^{-1}. Aerogel powders were mixed with potassium bromide (KBr) and pressed into pellets, which were outgassed at room temperature under a residual pressure of 0.1 Pa.

X-ray diffraction (XRD) patterns were obtained using a Panalytical X'Pert PRO diffractometer (Malvern Panalytical, Almelo, The Netherlands), equipped with Cu Kα radiation ($\lambda = 1.5406$ Å).

FESEM, FTIR, and XRD details are available in Appendix A supplementary file.

2.5 Statistical analysis

Data were expressed as the mean ± half-range uncertainty based on duplicate measurements from independent sample batches. Data reported without any uncertainty refers to single measurement.

3 Results and discussion

3.1 Effect of pH on hydrogel and aerogel appearance

Figure 2a reports the appearance of WPI hydrogels formed at pH values varying in the range 2–11 (protein concentration 20% (w/w), gelation temperature 90 °C, and heating time 30 min).

Hydrogels obtained at different gelation pH presented distinct visual differences in opacity and surface textures (Table 1).

WPI hydrogels produced at acidic gelation (pH ≤ 3) were transparent. The hydrogels gelled near the isoelectric point (pH 4–6) and exhibited an opaque white gel. Hydrogels formed at gelation neutral to slightly alkaline gelation (from pH 7 to 8.5) display white, compact, and homogeneous gels. Hydrogels gelled at high alkaline conditions exhibited a yellow hue.

These visual observations confirmed that pH is a primary determinant of WPI gelation chemistry. These appearance differences can be explained by considering the reactions occurring in the different pH ranges. Under acidic gelation conditions (pH ≤ 3), protonation occurs, which causes non-specific aggregation and increases intermolecular repulsion, resulting in weak structures that are prone to collapse [13].

Table 1 Physical appearance of WPI hydrogels and corresponding aerogels as a function of gelation pH

Gelation pH	Hydrogel appearance	Aerogel appearance
2	Transparent	Fractured, non-monolith
3	Transparent	Cracked monolith
4	Opaque white	White, smooth
5	Opaque white	White, smooth
6	White	White, smooth
7	White	White, smooth
7.5	White	White, smooth
8	Light white	White, smooth
8.5	Light white	White, smooth
9	Light white	White, smooth
10	Transparent	White, smooth
11	Yellowish transparent	White, smooth, translucent

As reported, gelation near the isoelectric point (pH 4–6) produced fine and more uniform protein networks supported by regulated self-assembly [27]. In this gelation pH region, the protein molecules carried minimal net surface charge. Thus, the isoelectric region facilitated rapid aggregation and formation of opaque particulate hydrogels due to limited electrostatic repulsion [37]. At neutral to slightly alkaline gelation pH conditions (pH 7-8.5), the electrostatic repulsion and thiol-disulfide crosslinking increased, resulting in a fine and homogeneous gel [38]. The yellow hue of hydrogels gelled at high alkaline conditions (pH ≥ 9) was caused by the formation of polysulfides from the β-elimination of cystine residues [39]. At alkaline conditions, intermolecular crosslinking and hydrophobic interactions induced the formation of stiff elastic gel networks [40].

The appearance of aerogels produced via $ScCO_2$ drying using precursor hydrogels gelled at pH (2–11) is reported in Fig. 2b. Aerogels produced from highly acidic gelation pH (pH ≤ 3) resulted in slightly transparent, cracked, and fragmented monoliths after $ScCO_2$ drying. AeroWPI-4, AeroWPI-5, and AeroWPI-6 appeared white and opaque, with a slightly dusty surface and a homogeneous structure. This appearance is likely due to a dense and compact structure with limited light transmission, typically observed near the isoelectric pH. As gelation pH increased, the aerogels AeroWPI-7 to AeroWPI-8.5 resulted in white and slightly brittle smooth-surface textured aerogels. Such an appearance may be attributed to a moderately porous structure with relatively uniform morphology. Aerogels produced at high alkaline gelation pH (pH ≥ 9) were white, smooth, and slightly translucent.

Aerogels produced under highly acidic gelation pH (pH ≤ 3) were broken and shattered due to capillary-induced collapse during solvent exchange [13]. Typically, acidic pH conditions cause high protonation and electrostatic repulsion and facilitate non-specific aggregation. These weak gel networks were unable to sustain capillary forces during solvent exchange [13].

At a gelation pH of 4–6 (near the isoelectric point of protein), dense particulate aggregation formed during gelation, and the resultant protein network was able to resist drying conditions [20, 37].

By increasing the pH to neutral or mildly alkaline (pH 7–8.5), the slight increase in electrostatic repulsion and thiol-disulfide crosslinking formed fine, elastic networks. These gel networks withstood the $ScCO_2$ drying conditions, resulting in porous aerogels [38]. These findings are supported by previous study outcomes where an optimal whey protein network was obtained at neutral pH. At this pH, the partial unfolding of proteins exposes reactive thiol groups while retaining enough electrostatic repulsion to avoid rapid aggregation [30]. According to the literature, at high alkaline gelation pH (pH ≥ 9), excessive protein unfolding causes over-crosslinking, which increases elasticity, resulting in smooth and brittle aerogels with diminished resistance [39].

Overall, these results showed the crucial role that gelation pH plays in regulating whey protein molecule assembly, which in turn controls the gel's macroscopic properties and the corresponding aerogel. This gelation-structure correlation may be significant for obtaining tunable aerogel properties for biomedical applications, including controlled porosity, mechanical stability, and absorption capacity [20, 41].

3.2 Effect of gelation pH on WPI aerogel physical properties

Table 2 shows the bulk density, porosity, and volume shrinkage of WPI aerogels. Aerogels produced from highly acidic gelation pH (≤ 3) showed the highest volume shrinkage (~ 50%) and density (0.39–0.47 g. cm^{-3}). The porosity of AeroWPI-2 was not measured because the samples were fragmented or broke during the liquid replacement. Aerogels produced from gelation pH 4–6 (AeroWPI-4, AeroWPI-5, AeroWPI-6) (close to the WPI isoelectric point) had moderate to high bulk density (0.24–0.28 g·cm^{-3}), moderate porosity (93–98%), and significant volume shrinkage (20–35%). At neutral to slightly alkaline gelation pH (7–8.5) (AeroWPI-7, AeroWPI-7.5, AeroWPI-8, AeroWPI-8.5), aerogel properties improved. This gelation range produced aerogels with the highest porosity (98–99%), low bulk density (0.23–0.25 g cm^{-3}), and moderate shrinkage (25–33%). Aerogels produced from gelation pH (≥ 9) exhibited a decreasing porosity from 96% (AeroWPI-9) to 48% (AeroWPI-11) as pH increased. The volume shrinkage was low (25–26%), and the density ranged between 0.14 g. cm^{-3} and 0.27 g. cm^{-3}.

Regarding the density of WPI aerogels, no clear evidence of a pH-dependent trend was observed.

Table 2 Physical properties of AeroWPI-2 to AeroWPI-11, ρ_b representing bulk density (g· cm^{-3}), ε representing porosity (%), and Sv for shrinkage volume (%)

Samples	ρ_b (g· cm^{-3})	ε (%)	S_v (%)
AeroWPI-2	0.47 ± 0.2	n.d	50 ± 20
AeroWPI-3	0.39 ± 0.3	41 ± 9	50 ± 20
AeroWPI-4	0.28 ± 0.1	93 ± 1	35 ± 7
AeroWPI-5	0.26 ± 0.1	98 ± 1	21 ± 10
AeroWPI-6	0.24 ± 0.1	94 ± 1	20 ± 20
AeroWPI-7	0.25 ± 0.1	98 ± 1	25 ± 11
AeroWPI-7.5	0.26 ± 0.1	99 ± 1	33 ± 12
AeroWPI-8	0.23 ± 0.1	98 ± 2	30 ± 12
AeroWPI-8.5	0.24 ± 0.1	98 ± 1	25 ± 11
AeroWPI-9	0.25 ± 0.1	96 ± 1	30 ± 10
AeroWPI-10	0.27 ± 0.1	88 ± 1	26 ± 11
AeroWPI-11	0.14 ± 0.1	48 ± 1	25 ± 7

Table 3 Textural properties of AeroWPI-2 to 11, SSA_{BET} = specific surface area, D_p = mean pore diameter, V_T = total pore volume

Samples	SSA_{BET} ($m^2 \cdot g^{-1}$)	D_p (nm)	V_T ($cm^3 \cdot g^{-1}$)
AeroWPI-2	96	10.2	0.28
AeroWPI-3	186	7.8	0.57
AeroWPI-4	100	20	0.32
AeroWPI-5	56	7.7	0.16
AeroWPI-6	21	10.9	0.05
AeroWPI-7	104	9.4	0.34
AeroWPI-7.5	107	10.5	0.35
AeroWPI-8	249	7.8	0.70
AeroWPI-8.5	312	9.8	1.02
AeroWPI-9	136	8.9	0.43
AeroWPI-10	196	7.4	0.53
AeroWPI-11	247	12.5	0.77

Some comments, however, can be made when considering porosity and shrinkage values. In highly acidic gelation conditions (pH ≤ 3), high protonation during the gelation phase results in electrostatic repulsion, which prevents the formation of a robust and cohesive protein network [42]. As a result, these gels further weaken during the solvent exchange steps, and the pores collapse during $ScCO_2$ drying, resulting in aerogels with limited porosity and high-volume shrinkage.

When gelation occurs near the isoelectric point (pH 4–6), proteins rapidly aggregate into dense, particulate networks with low elasticity [37]. These dense aggregations shrink during $ScCO_2$ drying due to capillary-induced stress and reduced internal-pore stability. This is consistent with a previously reported volume shrinkage of ~38–39% in WPI aerogels gelled at pH 4.8 [13, 43].

In the case of aerogels produced from neutral to slightly alkaline gelation pH (pH 7–8.5), the physical properties of WPI aerogels markedly improved. These properties are ascribed to an increase in electrostatic repulsion between partly deprotonated protein chains, which promotes the growth of fibrillar, fine-stranded gel networks that are structurally resistant to drying-induced collapse. Furthermore, under $ScCO_2$ drying conditions, the thiol-disulfide crosslinking stabilized the protein matrix, which allows the maintenance of an open porosity architecture [38, 40].

Aerogels produced from highly alkaline gelation pH (pH ≥ 9) exhibited a reduction in porosity. Highly alkaline conditions facilitate partial pore collapse and decrease aerogel homogeneity, due to disruption of the protein backbone [39]. Even though these aerogels exhibit low density at extremely alkaline pH (AeroWPI-11), they lack morphological homogeneity.

AeroWPI-7 and AeroWPI-8.5 showed optimal macroscopic characteristics, such as low density, high porosity, and minimum shrinkage, suggesting desired structural integrity and potential for biomedical applications, such as drug loading capacity and wound exudate absorption.

3.3 Effect of gelation pH on the textural properties of WPI-aerogel

Nitrogen adsorption-desorption analysis revealed the influence of gelation pH on textural properties of WPI aerogels, which are reported in Table 3.

Aerogels obtained under acidic conditions, AeroWPI-2 and AeroWPI-3, were characterized by moderate SSA (96, 186 $m^2 \cdot g^{-1}$, respectively). When increasing the gelation pH to values near the isoelectric point (pH ~ 4–6), a significant drop in SSA was observed, with values falling from 100 $m^2 \cdot g^{-1}$ (AeroWPI-4) to 21 $m^2 \cdot g^{-1}$ (AeroWPI-6). Gelation at neutral to mild alkaline pH (AeroWPI-7 to 8.5) leads to aerogels with a significantly increased SSA, reaching a maximum of 312 $m^2 \cdot g^{-1}$ for AeroWPI-8.5. The SSA decreased for aerogels produced at highly alkaline gelation conditions (pH ≥ 9), even though it increased again, reaching the value of 247 $m^2 \cdot g^{-1}$ for AeroWPI-11.

Concerning the total pore volume, a similar trend for SSA was observed (Table 3 and Fig. 3). AeroWPI-8.5 corresponded to the highest pore volume (1.02 $cm^3 \cdot g^{-1}$), while the lowest pore volume was observed near the isoelectric point for AeroWPI-6 (pore volume equal to 0.05 cm^3 g^{-1}).

Regarding the mean pore diameter, no similar trend was observed (Table 3 and Fig. 3). All aerogels showed an average pore diameter between 7 and 10 nm, except for AeroWPI-4 and AeroWPI-11, which displayed higher pore

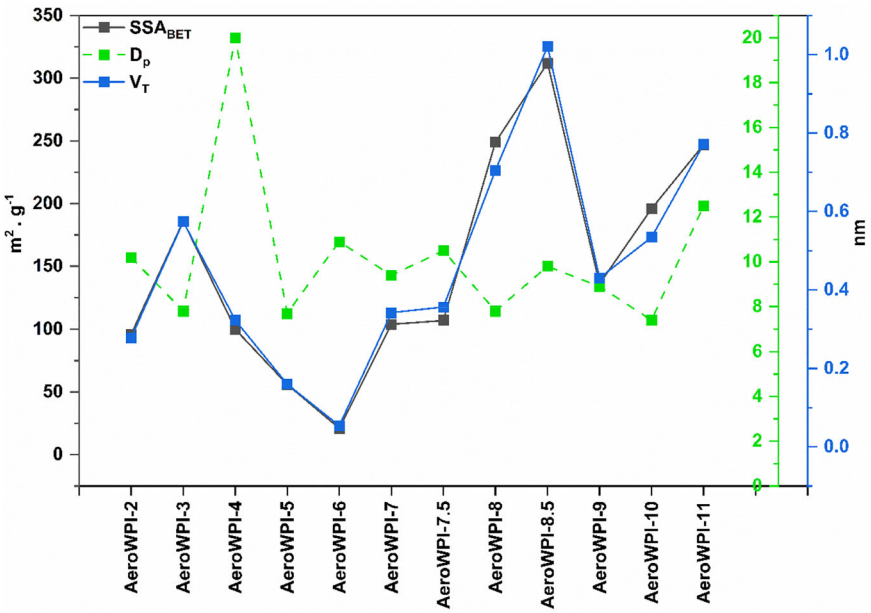

Fig. 3 Specific surface area (SSA_{BET}), pore diameter (D_p) and pore volume (V_{TP}) of aerogels produced at different gelation pH

diameters (20 and 13 nm, respectively). A previous study reported that WPI aerogels formed at gelation pH 3, 7, and 9 exhibited mesopore diameters ranging from 10 to 12.7 nm [40].

During the gelation at high acidic conditions, the formation of weakly interconnected aggregates was facilitated by protonation of amino groups to a large extent [39]. At this gelation pH, despite the formation of an initial porous network, a significant structural collapse may occur during $ScCO_2$ drying due to insufficient crosslinking, limiting the accessible mesoporous volume [44].

When gelation occurred near the isoelectric point (pH ~ 4–6), protein macromolecules had nearly negligible surface charge, which reduced electrostatic repulsions and enabled rapid aggregation into coarse particulate networks [45]. These particulate structures showed high shrinkage and reduced mesoporosity, which is consistent with previously reported results indicating that WPI aerogel gelled near pH 4.5 exhibited minimum surface area ($14 \pm 10\ m^2.\ g^{-1}$) and negligible pore volume, which was not determinable [20].

At neutral to mildly alkaline gelation pH (7–8.5), the formation of fine-stranded fibrillar networks stabilized by thiol-disulfide crosslinking and electrostatic repulsion increases the specific surface area and pore volume [40]. These structures facilitate the formation of high mesopore volume and interconnected pores, which may be resistant to capillary collapse during solvent exchange and $ScCO_2$ drying.

SSA and pore volume decreased under highly alkaline gelation conditions (pH ≥ 9), indicating the beginning of structural densification and pore collapse. This was consistent with alkaline-induced thiol-disulfide interchange reactions, which facilitate uncontrolled polymerization [44].

Overall, the correlation between SSA and pore volume versus gelation pH displayed a bimodal profile (Fig. 3), with a minimum for AeroWPI-6 ($21\ m^2.\ g^{-1}$ and $0.05\ cm^3.\ g^{-1}$) near the isoelectric point and a maximum for AeroWPI-8.5 ($312\ m^2.\ g^{-1}$ and $1.02\ cm^3.\ g^{-1}$) at mildly alkaline pH. These trends confirmed that the electrostatic interactions during gelation play a crucial role in governing the textural properties of protein-based aerogels [40].

3.4 Effect of gelation pH on surface charge and swelling properties of aerogels

The ζ-potential (reflecting the net electrokinetic charge) and swelling behavior of WPI aerogels as a function of gelation pH are reported in Fig. 4. Aerogels produced under acidic conditions (AeroWPI-2) exhibited a slightly positive ζ-potential (+4.6 mV). As the gelation pH increased toward the isoelectric point of WPI, the ζ-potential shifted from positive to negative values: AeroWPI-4 and AeroWPI-5 showed values of −13.5 mV and −36.8 mV, respectively. AeroWPI-7 and AeroWPI-7.5 showed ζ-potential values of −27.4 and −30.7 mV, respectively, while aerogels prepared at pH ≥ 8 (AeroWPI-8) showed ζ-potential near zero (−0.4 to 0.3 mV).

The slightly positive ζ-potential (+4.6 mV) exhibited by AeroWPI-2 (at highly acidic gelation pH) is attributed to the positively charged amino groups ($-NH_3^+$) on the surface [44]. With increasing pH below the isoelectric point (AeroWPI-4 to AeroWPI-5), deprotonation of carboxyl groups occurs, forming negatively charged groups ($-COO^-$), which causes a decrease in the total charge [46]. The ζ-potential values of AeroWPI-6 approaching zero indicated reduced net surface charge of aerogel; however, this should not be interpreted as the isoelectric point of native WPI, which may be altered by

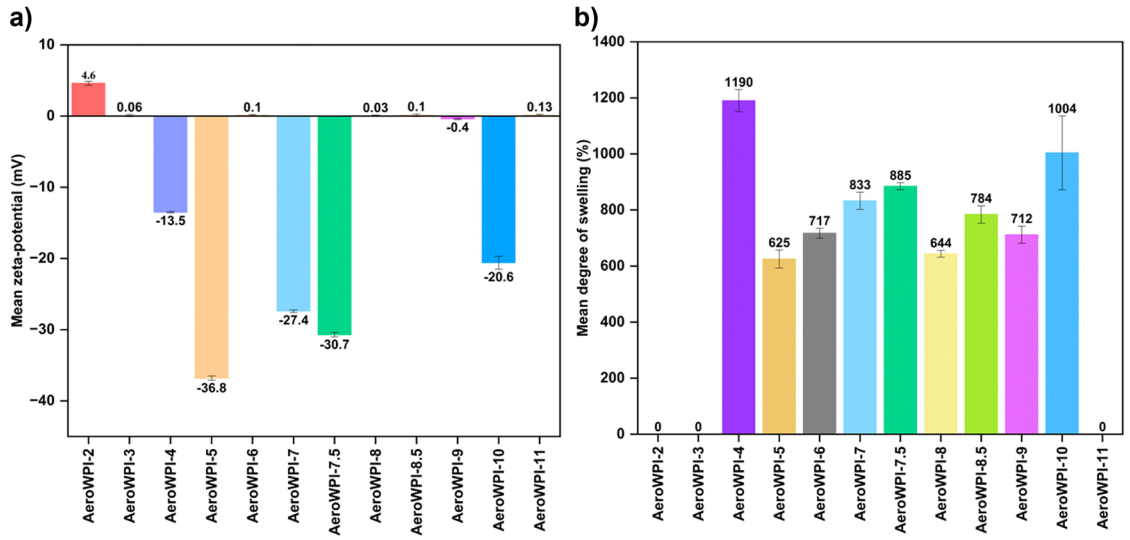

Fig. 4 Aerogels mean zeta potential (**a**) and mean degree of swelling (**b**)

protein denaturation, aggregation, solvent exchange, and $ScCO_2$ drying.

Gelation at pH 7–7.5 (AeroWPI-7 and AeroWPI-7.5) caused a decrease in ζ-potential values of aerogels (−27.4 to −30.7 mV). These negative values were due to the exposure of buried charged groups resulting from the partial unfolding of proteins induced by the heat-denaturation process (90 °C for 30 min) [47]. At alkaline gelation conditions (pH ≥ 8), the increase in disulfide crosslinking and β-elimination processes decreases the ionizable residues available for charge generation [48], resulting in a zeta-potential close to zero. AeroWPI-10 showed a negative zeta-potential, which may be tentatively attributed to the combination of charge shielding or partial masking of ionizable groups during the solvent exchange and $ScCO_2$ drying process [49].

Figure 4b reports the swelling behavior of aerogels prepared at varying gelation pH values. Aerogels from AeroWPI-5 to AeroWPI-9 presented average swelling values in the range of 625–885%. The degree of swelling increases from pH 5 to pH 7.5, after which it decreases as the gelation conditions move towards more alkaline (AeroWPI-9). This trend is similar to the trend observed for the values of *SSA*, V_T, and ε (Fig. 3 and Tables 2 and 3). This result suggested that the swelling degree was affected by the textural properties of the aerogels, which in turn were influenced by the gelation pH. This is in accordance with the literature, where polymeric porous systems with high porosity and pore connectivity were reported to have higher swelling ratios [50].

The AeroWPI-4 and AeroWPI-10 exhibited significantly higher swelling values (1000–1190%), deviating from the overall trend. A similar behavior is reported in the literature, where WPI aerogels gelled at pH 10 showed a higher swelling degree than the samples gelled at neutral pH [20]. The high swelling degree obtained from AeroWPI-4 may be due to the bigger pore dimension displayed by this sample (Table 3 and Fig. 3). Overall, the degree of swelling may also be linked to the crosslinking density of the polymer network [51]. Therefore, it cannot be ruled out that the exceptional values observed for AeroWPI-4 and AeroWPI-10 were due to a lower crosslinking density. Finally, samples AeroWPI-2, AeroWPI-3, and AeroWPI-11 disintegrated and lost their shape during the swelling test.

To conclude, all the swelling ratios observed for the AeroWPI-5 to AeroWPI-9 were in line, if not superior, with those reported in the literature for WPI films for wound dressing or packaging (210% [52] and 140% [53]). In addition, the aerogels obtained in our work display higher degrees of swelling than those of WPI aerogels for drug delivery from previous studies (250%) [20].

3.5 Influence of gelation pH on WPI aerogel liquid absorption capacity

The liquid absorption capacity of WPI aerogels in PBS is reported in Fig. 5. Overall, the absorption capacity of aerogels, between AeroWPI-4 and AeroWPI-10, ranged from 380% to 800%. These values are comparable to those reported in the literature for similar systems. In particular, aerogel/hydrogel biphasic gels made of lactoglobulin and polyvinyl alcohol for wound dressing were reported to have absorption capacities in PBS between 600% and 800% [54]. This confirmed that the absorption properties of the aerogels synthesized in our work are comparable to previous systems and relevant for wound applications.

A recent study reported the high absorption capacity (~4282%) and water retention (~73%) of porous Kaolin/chitin composite aerogel, which exhibited an excellent hemostatic effect [55].

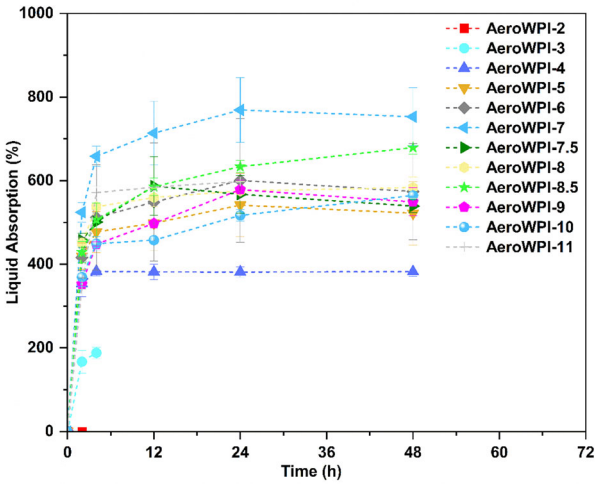

Fig. 5 Liquid absorption capacity (%) of aerogels

The highest absorption capacity was obtained for the AeroWPI-7 aerogel. This may be explained by the fact that this sample presented relatively high swelling degree, SSA, pore volume, and porosity. In contrast, the lowest absorption capacity was observed for the AeroWPI-4 aerogel. It must be noted that this sample was likely to have a low crosslinking degree (as suggested by the swelling results, Fig. 4b). This may cause a partial dissolution of the protein matrix during the absorption test in PBS, leading to an underestimation of its absorption capacity. Finally, AeroWPI-2, AeroWPI-3, and AeroWPI-11 aerogels disintegrated during the absorption test in PBS, analogously to what was observed during the swelling analysis.

4 Conclusion

In this work, the effect of gelation pH on the final properties of the resulting whey protein isolate (WPI) aerogels was systematically studied. Variations in density, porosity, surface area, swelling, ζ-potential, and absorption behavior have shown that the gelation pH affected the molecular assembly, network formation, and ultimate aerogel performance. Aerogels prepared near the WPI isoelectric point (pH 4–6) exhibited compact particulate networks with high density and low porosity. This structure indicates limited network flexibility and uncontrolled aggregation, resulting in reduced absorption capacity. In contrast, gelation at neutral to mildly alkaline conditions (pH 7–8.5) favored thiol-mediated self-assembly and electrostatic stabilization, resulting in highly porous, fine-stranded structures. This gelation pH range resulted in aerogels with optimal surface area (104–312 m^2/g), ζ-potential (−27.4–0.1 mV), high swelling capacity (784–833%), and structural integrity. Aerogels produced from more alkaline gelation pH ≥ 9 showed a decrease in surface area and absorption capacity, as well as a tendency to lose structural integrity in PBS and water. This behavior may be attributed to the over-crosslinking observed in highly alkaline conditions.

Considering a possible application of WPI aerogels for wound treatment, absorption capacity stands out as a crucial property. From this perspective, the aerogels gelled at pH 7 presented an excellent absorption capacity. This property arises from the relatively high values of SSA, pore volume, and porosity of these aerogels, which, in turn, stem from a good compromise of interactions between proteins during gelation at pH 7.

To conclude, this study highlights pH modulation as a straightforward and effective strategy for modifying aerogel properties and performance without the use of hazardous chemical crosslinkers. WPI aerogels showed potential as next-generation biomaterials for chronic wound treatment, tissue engineering scaffolds, and drug delivery platforms. To further explore their clinical translation, future research will concentrate on integrating bioactive substances into the WPI network and evaluating their biological performance. Overall, this study provides directions for the design of sustainable protein-based biomaterials by systematically connecting gelation conditions, protein chemistry, and aerogel performance.

Data availability

Data will be made available on request.

Supplementary information The online version contains supplementary material available at https://doi.org/10.1007/s10971-026-07221-0.

Acknowledgements The authors thank Milei® GmbH (Leutkirch, Germany) for kindly supplying all the WPI used for this study.

Author contributions UA: Original draft writing, Investigation, Data curation; MG: Investigation, Methodology, Data curation, Writing—review and editing; LM: experimental methodology, Supervision; FB: Supervision, Writing—review; BO: Methodology, Writing—review and editing, Conceptualization, Supervision, Funding acquisition.

Funding This project is supported by "European Union Next-Generation EU (PIANO NAZIONALE DI RIPRESA E RESILIENZA (PNRR), Italy". The activity concerns the PNRR missions "Emerging infectious diseases", "Diagnostics and innovative therapies in precision medicine" and "Consequences and challenges of aging". Open access funding provided by Politecnico di Torino within the CRUI-CARE Agreement.

Compliance with ethical standards

Conflict of interest The authors declare no competing interests.

Publisher's note Springer Nature remains neutral with regard to jurisdictional claims in published maps and institutional affiliations.

References

1. Leite AC, Pereira RN, Rodrigues RM (2025) Protein aerogels as food-grade delivery systems—a comprehensive review. Food Hydrocoll 163: 111138 https://doi.org/10.1016/j.foodhyd.2025.111138
2. Soorbaghi FP, Isanejad M, Salatin S, Ghorbani M, Jafari S, Derakhshankhah H (2019) Bioaerogels: synthesis approaches, cellular uptake, and biomedical applications. Biomed Pharmacother 111:964–975 https://doi.org/10.1016/j.biopha.2019.01.014
3. García-González CA, Blanco-Vales M, Barros J, Boccia AC, Budtova T, Durães L, Erkey C, Gallo M, Herman P, Kalmár J, Iglesias-Mejuto A, Malfait WJ, Zhao S, Manzocco L, Plazzotta S, Milovanovic S, Neagu M, Nita LE, Paraskevopoulou P, Roig A, Simón-Vázquez R, Smirnova I, Tomović Ž, López-Iglesias C (2025) Review and perspectives on the sustainability of organic aerogels. ACS Sustain Chem Eng 13:6469–6492
4. Gou D, Ren P, Ren F, Wang Q, Zhang H, Cheng X, Wang L, Liu T, Zhao J (2025) Fabrication, characterization and food applications of multifunctional chitosan-based aerogels: a review. Int J Biol Macromol 320: 145702 https://doi.org/10.1016/j.ijbiomac.2025.145702
5. Karamikamkar S, Yalcintas EP, Haghniaz R, de Barros NR, Mecwan M, Nasiri R, Davoodi E, Nasrollahi F, Erdem A, Kang H, Lee J, Zhu Y, Ahadian S, Jucaud V, Maleki H, Dokmeci MR, Kim HJ, Khademhosseini A (2023) Ali, aerogel-based biomaterials for biomedical applications: from fabrication methods to disease-targeting applications. Adv Sci 10:e2204681-NA https://doi.org/10.1002/advs.202204681
6. Liu Z, Ran Y, Xi J, Wang J (2020) Polymeric hybrid aerogels and their biomedical applications. Soft Matter 16:9160–9175 https://doi.org/10.1039/d0sm01261k
7. Guastaferro M, Reverchon E, Baldino L (2021) Polysaccharide-based aerogel production for biomedical applications: a comparative review. Materials 14:1631 https://doi.org/10.3390/ma14071631
8. Peng J, Xiao Q, Xue J, Cao Y, Chen J, Zhao J, Ding Y, Yang X, Yang Y (2025) Chitosan/polyvinyl alcohol aerogels with improved structure for thermal insulation and noise reduction. Int J Biol Macromol 323: 147175 https://doi.org/10.1016/j.ijbiomac.2025.147175
9. Chu S, Wang AL, Bhattacharya A, Montclare JK (2021) Protein-based biomaterials for therapeutic and diagnostic applications. Prog Biomed Eng 4:012003 https://doi.org/10.1088/2516-1091/ac2841
10. Hu Z, Cao W, Shen L, Sun Z, Yu K, Zhu Q, Ren T, Zhang L, Zheng H, Gao C, He Y, Guo C, Zhu Y, Ren D (2022) Scalable milk-derived whey protein hydrogel as an implantable biomaterial. ACS Appl Mater Interfaces 14:28501–28513 https://doi.org/10.1021/acsami.2c02361
11. Farooq MA, Aquib M, Ghayas S, Bushra R, Haleem Khan D, Parveen A, Wang B (2019) Whey protein: a functional and promising material for drug delivery systems recent developments and future prospects. Polym Adv Technol 30:2183–2191 https://doi.org/10.1002/pat.4676
12. Dziadek M, Charuza K, Kudlackova R, Aveyard J, D'Sa R, Serafim A, Stancu I-C, Iovu H, Kerns JG, Allinson S, Dziadek K, Szatkowski P, Cholewa-Kowalska K, Bacakova L, Pamula E, Douglas TEL (2021) Modification of heat-induced whey protein isolate hydrogel with highly bioactive glass particles results in promising biomaterial for bone tissue engineering. Mater Des 205: 109749 https://doi.org/10.1016/j.matdes.2021.109749
13. Manzocco L, Plazzotta S, Powell J, de Vries A, Rousseau D, Calligaris S (2022) Structural characterisation and sorption capability of whey protein aerogels obtained by freeze-drying or supercritical drying. Food Hydrocoll 122: 107117 https://doi.org/10.1016/j.foodhyd.2021.107117
14. Plazzotta S, Alongi M, Berardinis LD, Melchior S, Calligaris S, Manzocco L (2022) Steering protein and lipid digestibility by oleogelation with protein aerogels. Food Funct 13:10601–10609 https://doi.org/10.1039/D2FO01257J
15. Plazzotta S, Calligaris S, Manzocco L (2020) Structural characterization of oleogels from whey protein aerogel particles. Food Res Int 132: 109099 https://doi.org/10.1016/j.foodres.2020.109099
16. Zhou X, Guo X, Chai Y, Li X, Chen L, Feng X (2024) Superabsorbent whey protein isolates/chitosan-based antibacterial aerogels: preparation, characterization and application in chicken meat preservation. Int J Biol Macromol 259: 128961 https://doi.org/10.1016/j.ijbiomac.2023.128961
17. Effraimopoulou E, Kalmár J, Paul G, Marchese L, Ioannou D, Paraskevopoulou P, Gurikov P (2024) Whey protein isolate-based aerogels with improved hydration properties for food packaging applications. ACS Appl Nano Mater 7:618–627 https://doi.org/10.1021/acsanm.3c04784
18. Lovskaya D, Bezchasnyuk A, Mochalova M, Tsygankov P, Lebedev A, Zorkina Y, Zubkov E, Ochneva A, Gurina O, Silantyev A, Majouga A, Menshutina N (2022) Preparation of protein aerogel particles for the development of innovative drug delivery systems. Gels 8:765 https://doi.org/10.3390/gels8120765
19. Kieserling H, Heine J, Schroeter B, Drusch S, Maares M, Rohn S, Haase H, Gurikov P, Keil C (2026) Whey protein-based aerogels: structural insights, zinc-carrier properties, and zinc bioavailability in Caco-2 cells. Food Hydrocoll 172: 112163 https://doi.org/10.1016/j.foodhyd.2025.112163
20. Betz M, García-González CA, Subrahmanyam RP, Smirnova I, Kulozik U (2012) Preparation of novel whey protein-based aerogels as drug carriers for life science applications. J Supercrit Fluids 72:111–119 https://doi.org/10.1016/j.supflu.2012.08.019
21. Nyström G, Fong W-K, Mezzenga R (2017) Ice-templated and cross-linked amyloid fibril aerogel scaffolds for cell growth. Biomacromolecules 18:2858–2865 https://doi.org/10.1021/acs.biomac.7b00792
22. Wang J, Niu J, Ji H, Li X, McClements DJ, Jin Z, Jiang L, Wen J, Qiu C (2024) Regulation of adsorption properties of whey protein isolate fibril–calcium alginate aerogels by controlling protein fibrillation time. Langmuir 40:23230–23242 https://doi.org/10.1021/acs.langmuir.4c02474
23. Tu J-L, Lai Y-R, Lin C-Y, Wang SS-S, Lin T-H (2024) Applications of three-dimensional whey protein amyloid fibril-based hybrid aerogels in oil/water separation and emulsion separation. Int J Biol Macromol 283: 137680 https://doi.org/10.1016/j.ijbiomac.2024.137680
24. RS Pires, AJ Capezza, D Jonsson, JL Morén, MS Hedenqvist, C Lendel, Elucidating the role of the nanostructure in protein aerogels for removal of organic water pollutants, 2024. https://doi.org/10.1039/D4SU00352G

25. Tang Q, Roos YH, Miao S (2024) Structure, gelation mechanism of plant proteins versus dairy proteins and evolving modification strategies. Trends Food Sci Technol 147: 104464 https://doi.org/10.1016/j.tifs.2024.104464
26. Andlinger DJ, Bornkeßel AC, Jung I, Schroeter B, Smirnova I, Kulozik U (2021) Microstructures of potato protein hydrogels and aerogels produced by thermal crosslinking and supercritical drying. Food Hydrocoll 112: 106305 https://doi.org/10.1016/j.foodhyd.2020.106305
27. Tang Q, Roos YH, Miao S (2024) Comparative studies of structural and thermal gelation behaviours of soy, lentil and whey protein: a pH-dependency evaluation. Food Hydrocoll 146: 109240 https://doi.org/10.1016/j.foodhyd.2023.109240
28. Wijayanti HB, Bansal N, Deeth HC (2014) Stability of whey proteins during thermal processing: a review. Compr Rev Food Sci Food Saf 13:1235–1251 https://doi.org/10.1111/1541-4337.12105
29. Nicolai T (2019) Gelation of food protein–protein mixtures. Adv Colloid Interface Sci 270:147–164 https://doi.org/10.1016/j.cis.2019.06.006
30. Lazidis A, Hancocks RD, Spyropoulos F, Kreuß M, Berrocal R, Norton IT (2016) Whey protein fluid gels for the stabilisation of foams. Food Hydrocoll 53:209–217 https://doi.org/10.1016/j.foodhyd.2015.02.022
31. Wen-qiong W, Pei-pei Y, Ji-yang Z, Zhi-hang G (2021) Effect of temperature and pH on the gelation, rheology, texture, and structural properties of whey protein and sugar gels based on Maillard reaction. J Food Sci 86:1228–1242 https://doi.org/10.1111/1750-3841.15659
32. Wang Y, Zhao J, Zhang W, Liu C, Jauregi P, Huang M (2020) Modification of heat-induced whey protein gels by basic amino acids. Food Hydrocoll 100: 105397 https://doi.org/10.1016/j.foodhyd.2019.105397
33. Nicolai T, Durand D (2013) Controlled food protein aggregation for new functionality. Curr Opin Colloid Interface Sci 18:249–256 https://doi.org/10.1016/j.cocis.2013.03.001
34. He Z, Ma T, Zhang W, Su E, Cao F, Huang M, Wang Y (2021) Heat-induced gel formation by whey protein isolate-*Lycium barbarum* polysaccharides at varying pHs. Food Hydrocoll 115: 106607 https://doi.org/10.1016/j.foodhyd.2021.106607
35. Kleemann C, Schuster R, Rosenecker E, Selmer I, Smirnova I, Kulozik U (2020) In-vitro-digestion and swelling kinetics of whey protein, egg white protein and sodium caseinate aerogels. Food Hydrocoll 101: 105534 https://doi.org/10.1016/j.foodhyd.2019.105534
36. Thommes M, Kaneko K, Neimark AV, Olivier JP, Rodriguez-Reinoso F, Rouquerol J. KSW Sing, Physisorption of gases, with special reference to the evaluation of surface area and pore size distribution (IUPAC Technical Report), 2015 https://www.degruyterbrill.com/document/doi/10.1515/pac-2014-1117/html.
37. Stading M, Hermansson A-M (1990) Viscoelastic behaviour of β-lactoglobulin gel structures. Food Hydrocoll 4:121–135 https://doi.org/10.1016/S0268-005X(09)80013-1
38. Li H, Chen XD, Mercadé-Prieto R (2017) Elastic modulus and equilibrium swelling of stranded and particulate protein hydrogels at acid pH. Food Hydrocoll 71:168–175 https://doi.org/10.1016/j.foodhyd.2017.05.008
39. Fan L, Ge A, Chen XD, Mercadé-Prieto R (2019) The role of non-covalent interactions in the alkaline dissolution of heat-set whey protein hydrogels made at gelation pH 2–11. Food Hydrocoll 89:100–110 https://doi.org/10.1016/j.foodhyd.2018.10.035
40. Jung I, Schroeter B, Plazzotta S, De Berardinis L, Smirnova I, Gurikov P, Manzocco L (2023) Oleogels from mesoporous whey and potato protein-based aerogel microparticles: influence of microstructural properties on oleogelation ability. Food Hydrocoll 142: 108758 https://doi.org/10.1016/j.foodhyd.2023.108758
41. Bernardes BG, Del Gaudio P, Alves P, Costa R, García-Gonzaléz CA, Oliveira AL (2021) Bioaerogels: promising nanostructured materials in fluid management, healing and regeneration of wounds. Molecules 26:3834–3862 https://doi.org/10.3390/molecules26133834
42. Turgeon SL, Beaulieu M (2001) Improvement and modification of whey protein gel texture using polysaccharides. Food Hydrocoll 15:583–591 https://doi.org/10.1016/S0268-005X(01)00064-9
43. De Berardinis L, Plazzotta S, Magnan M, Manzocco L (2024) Hybrid aerogels of spirulin and whey proteins as novel cellular solids. LWT 213: 117078 https://doi.org/10.1016/j.lwt.2024.117078
44. Peydayesh M, Boschi E, Bagnani M, Tay D, Donat F, Almohammadi H, Li M, Usuelli M, Shiroka T, Mezzenga R (2024) Hybrid amyloid–chitin nanofibrils for magnetic and catalytic aerogels. ACS Nano 18:6690–6701 https://doi.org/10.1021/acsnano.4c00883
45. Young PW, Mills TB, Norton IT (2021) Influence of pH on fluid gels produced from egg and whey protein isolate. Food Hydrocoll 111: 106108 https://doi.org/10.1016/j.foodhyd.2020.106108
46. Ravindran S, Williams MAK, Ward RL, Gillies G (2018) Understanding how the properties of whey protein stabilized emulsions depend on pH, ionic strength and calcium concentration, by mapping environmental conditions to zeta potential. Food Hydrocoll 79:572–578 https://doi.org/10.1016/j.foodhyd.2017.12.003
47. Mohammadian M, Salami M, Emam-Djomeh Z, Momen S, Moosavi-Movahedi AA (2018) Gelation of oil-in-water emulsions stabilized by heat-denatured and nanofibrillated whey proteins through ion bridging or citric acid-mediated cross-linking. Int J Biol Macromol 120:2247–2258 https://doi.org/10.1016/j.ijbiomac.2018.08.085
48. Meng Y, Zhao X, Jiang Y, Ban Q, Wang X (2023) Effect of Maillard reaction conditions on the gelation and thermal stability of whey protein isolate/d-tagatose conjugates. Food Chem 405: 134928 https://doi.org/10.1016/j.foodchem.2022.134928
49. Kleemann C, Selmer I, Smirnova I, Kulozik U (2018) Tailor-made protein-based aerogel particles from egg white protein, whey protein isolate and sodium caseinate: influence of the preceding hydrogel characteristics. Food Hydrocoll 83:365–374 https://doi.org/10.1016/j.foodhyd.2018.05.021
50. Alsaid Y, Wu S, Wu D, Du Y, Shi L, Khodambashi R, Rico R, Hua M, Yan Y, Zhao Y, Aukes D, He X (2021) Tunable sponge-like hierarchically porous hydrogels with simultaneously enhanced diffusivity and mechanical properties. Adv Mater 33: 2008235 https://doi.org/10.1002/adma.202008235
51. Betz M, Hörmansperger J, Fuchs T, Kulozik U. Swelling behaviour, charge and mesh size of thermal protein hydrogels as influenced by pH during gelation. 2012 https://doi.org/10.1039/C2SM06976H
52. Schmid M, Prinz TK, Müller K, Haas A (2017) UV radiation-induced cross-linking of whey protein isolate-based films. Int J Polym Sci 2017: 1846031 https://doi.org/10.1155/2017/1846031
53. Pino P, Ronchetti S, Mollea C, Sangermano M, Onida B, Bosco F. Whey proteins–zinc oxide bionanocomposite as antibacterial films. Pharmaceutics 2021 https://www.mdpi.com/1999-4923/13/9/1426
54. Gong M, Shi H, Hu Z, Wang F, Dong M, Lei R, Zeng Z, Wang Y, Chen J (2023) Aerogel-hydrogel biphase gels based on physically crosslinked β-lactoglobulin fibrils/polyvinyl alcohol for skin wound dressings: in vitro and in vivo characterization. Chem Eng J 473: 145394 https://doi.org/10.1016/j.cej.2023.145394
55. He M, Huang Y, Cui Z, Cheng Z, Cao W, Wang G, Yao W, Feng M (2026) Construction of flexible kaolin/chitin composite aerogels and their properties. Gels 12:76 https://doi.org/10.3390/gels12010076